

Orbital order, anisotropic spin couplings, and the spin-wave spectrum of the ferromagnetic Mott insulator YTiO_3

Robert Schmitz,^{1,2} Ora Entin-Wohlman,² Amnon Aharony,² and Erwin Müller-Hartmann¹

¹*Institut für Theoretische Physik, Universität zu Köln, Zùlpicher Straße 77, 50937 Köln, Germany*

²*School of Physics and Astronomy, Raymond and Beverly Sackler*

Faculty of Exact Sciences, Tel Aviv University, Tel Aviv 69978, Israel

(Dated: September 10, 2018)

Using a point-charge calculation of the electrostatic crystal field, we determine the non-degenerate orbital ground state of the ferromagnetic Mott insulator YTiO_3 , which is found to agree perfectly with experiment. Based on the orbital order, we obtain by perturbation theory an effective spin Hamiltonian that describes the magnetic superexchange between nearest-neighbor Ti ions. The superexchange Hamiltonian includes, in addition to the isotropic Heisenberg coupling, antisymmetric (Dzyaloshinskii-Moriya) and symmetric anisotropy terms, caused by the spin-orbit interaction on the Ti ions. We find ferromagnetic Heisenberg couplings for Ti-Ti bonds in the crystallographic ab planes, but antiferromagnetic ones for Ti-Ti bonds between planes, in contradiction with experiment (which gives ferromagnetic couplings for both). Difficulties in calculating realistic values for the isotropic couplings of YTiO_3 have been already reported in the literature. We discuss possible origins for these discrepancies. However, the much smaller values we obtain for the symmetric and antisymmetric anisotropies may be expected to be reliable. We therefore combine the experimentally-deduced isotropic coupling with the calculated anisotropic ones to determine the magnetic order of the Ti ions, which is found to be in satisfactory agreement with experiment. Based on this magnetic order, we derive the spin-wave spectrum. We find an acoustic branch with a very small zone-center gap and three optical spin-wave modes with sizeable zone-center gaps. The acoustic branch reproduces the one reported in experiment, and the optical ones are in a satisfactory agreement with experiment, upon a proper folding of the magnetic Brillouin zone.

PACS numbers: 71.10.-w, 71.27.+a, 75.10.Dg, 75.25.+z, 75.30.Dg

I. INTRODUCTION

The perovskite Ti oxides have attracted much interest since these strongly-correlated electronic systems possess orbital and magnetic degrees of freedom which are coupled together (for a review, see Ref. [1]). A prominent member of this family is the *ferromagnetic* Mott insulator YTiO_3 . The Curie temperature of this compound is $T_C = 30$ K and the ordered ferromagnetic moment, which is oriented along the crystallographic c axis, is $0.84 \mu_B$ [2]. Another experiment [3] reported $T_C = 27$ K. Due to spin canting, there are also a small G-type antiferromagnetic moment along the a axis and a small A-type one along the b axis, which at $T = 10$ K amount to $0.08 \mu_B$ and $0.05 \mu_B$, respectively (the c -axis ferromagnetic moment being $0.54 \mu_B$ at that temperature, which is extrapolated to $0.72 \mu_B$ at zero temperature) [3].

Several previous calculations aiming to explain YTiO_3 and the doped series $\text{La}_{1-x}\text{Y}_x\text{TiO}_3$, respectively, have failed to achieve a consistent description of the experimentally observed orbital and magnetic ordering [3, 4, 5, 6]. A recent GGA+U (generalized gradient approximation + local Coulomb repulsion) study [7] has produced the correct orbital and magnetic ground state of YTiO_3 , but has not provided quantitative estimates for the superexchange couplings between nearest-neighbor Ti ions. These couplings are required in order to understand quantitatively the magnetic structure and the spin-wave spectrum observed in experiment [3].

From the microscopic point of view, YTiO_3 is quite

similar to the *antiferromagnetic* Mott insulator LaTiO_3 : In both compounds there is a single electron in the $3d$ shell of Ti, and both have the same space group, $Pbnm$. It is worth noting in this connection that the magnetic structure of LaTiO_3 is also quite complicated: Experiment has indicated a predominant antiferromagnetic G-type moment along the a axis and a small ferromagnetic moment along the c axis [8], and a recent theory [9] has predicted a small A-type moment along the b axis. We have recently presented a detailed model for LaTiO_3 [9], which proved successful in describing the orbital and magnetic ordering of that material and provided the superexchange couplings and the spin-wave dispersion measured in experiment [10]. Because of the apparent similarity between YTiO_3 and LaTiO_3 , one may hope that the same model will explain the former as well. In this paper we carry out such investigation. Unfortunately, our model does not yield the correct isotropic Heisenberg superexchange coupling between nearest-neighbor Ti ions. The reason is that there are both ferromagnetic and antiferromagnetic contributions to that coupling, which have roughly the same order of magnitude. Our approximations cannot resolve the competition between them to a sufficient precision. A similar problem has been reported in Ref. [3].

Superexchange couplings are customarily derived perturbatively, assuming that the hopping matrix elements are smaller than the on-site excitation energies. It has been found in other systems [11] that such calculations yield inaccurate values for the leading Heisen-

berg (isotropic) couplings, but are quite reliable for the much smaller anisotropic ones. It seems therefore reasonable to combine the experimental information on the isotropic couplings together with the calculated values of the anisotropic ones, in order to determine the magnetic structure of the ground state and the spin excitations. This procedure will be adopted in this paper.

We begin in Sec. II with a point-charge calculation of the electrostatic crystal field due to all ions of the solid. The ground state of this crystal field determines the orbital order of the Ti ions. This orbital ordering agrees extremely well with the one detected experimentally [12, 13]. We then use a Slater-Koster parametrization to compute the effective Ti-Ti hopping matrix elements. The Coulomb correlations on the doubly occupied d shells are fully taken into account in terms of Slater integrals. Having thus obtained an effective microscopic Hamiltonian for the Ti ions, we derive in Sec. III the superexchange spin couplings between nearest-neighbor Ti ions, employing perturbation theory to leading (second) order in the hopping matrix elements, and up to second order in the spin-orbit interaction on the Ti's. In this way we obtain, beside the isotropic superexchange coupling alluded to above, the antisymmetric (Dzyaloshinskii-Moriya) and symmetric superexchange anisotropies. Replacing the isotropic coupling by the experimentally-determined one, we calculate in Sec. IV the magnetic order of the classical ground state of the Ti ions and in Sec. V the spin-wave spectrum. The magnetic structure of the classical ground state is shown to be in satisfactory agreement with experiment [3]. The spin-wave calculation reproduces an acoustic branch of the spin-wave dispersion which has been detected by neutron scattering [3]. This branch has a very small zone-center gap, and is almost isotropic in the magnetic Brillouin zone. In addition, we identify three optical spin-wave branches with considerable zone-center gaps. The experimental dispersion has been plotted as a single branch over the magnetic Brillouin zone (MBZ) of a pure ferromagnet [3]. However, YTiO_3 is a *canted* ferromagnet, for which the MBZ is four times smaller. We therefore prefer to re-plot the experimental spin-wave data according to the actual MBZ, i. e., to fold back the experimental data from the MBZ of the purely ferromagnetic case. When this procedure is adopted, one obtains a satisfactory agreement between the optical branches and experiment. In Sec. VI we summarize our results and compare our picture of YTiO_3 with the ones given previously in the literature [3, 4, 5, 6].

II. THE MODEL

A. The crystal field

As is mentioned above, there is a single electron in the $3d$ shell of the Ti ions in the ground state (YTiO_3 has the valences $\text{Y}^{3+}\text{Ti}^{3+}(\text{O}^{2-})_3$). The unit cell, shown in Fig. 1,

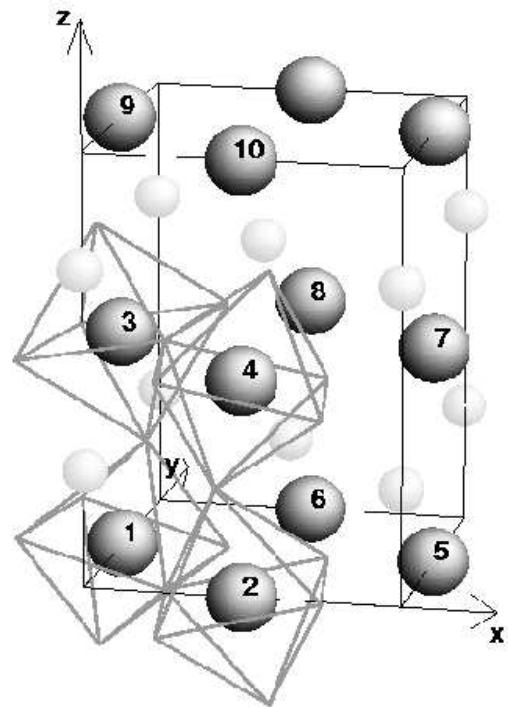


FIG. 1: The crystallographic structure of YTiO_3 . The ten Ti ions, which constitute the twelve inequivalent nearest-neighbor Ti-Ti bonds are enumerated. For simplicity, oxygen octahedra are only shown around four Ti sites. Y ions from two layers are shown as small spheres.

TABLE I: The structural parameters of YTiO_3 at $T = 2$ K [15].

a	5.32260 Å	$x_{\text{O}1}$	0.12133
b	5.69517 Å	$y_{\text{O}1}$	0.45702
c	7.59622 Å	$x_{\text{O}2}$	0.69010
x_{Y}	0.97762	$y_{\text{O}2}$	0.30919
y_{Y}	0.07398	$z_{\text{O}2}$	0.05770

contains four Ti ions and twelve inequivalent nearest-neighbor Ti-Ti bonds. The crystal has the symmetry of the space group $Pbnm$ (No. 62 in Ref. [14]). The structural data (taken at $T = 2$ K) are given in Table I [15]. In order to use the symmetries of the space group, it is convenient to employ the orthorhombic orthonormal basis for the Ti- d orbitals,

$$|xy\rangle, |2z^2\rangle, |yz\rangle, |xz\rangle, |x^2 - y^2\rangle, \quad (1)$$

where the x , y and z axes correspond to the crystallographic a , b and c axes.

Using the structural data listed in Table I, we have calculated the spectrum and the eigenstates of Ti ion No. 1 (see Fig. 1), employing a point-charge calculation of the static crystal-field Hamiltonian. This calculation uses the full Madelung sum over the crystal, which is evaluated as an Ewald sum [16]. It requires the second

TABLE II: The static crystal field for Ti^{3+} (site 1): Spectrum and eigenstates in the orthorhombic basis for the d basis, see Eq. (1).

-0.458 eV	(-0.181, 0.295, 0.488, -0.542, 0.590)
-0.308 eV	(-0.081, -0.412, 0.529, 0.653, 0.343)
-0.181 eV	(0.444, 0.266, 0.654, -0.017, -0.552)
0.407 eV	(0.761, 0.302, -0.231, 0.222, 0.477)
0.540 eV	(-0.430, 0.762, -0.039, 0.480, -0.040)

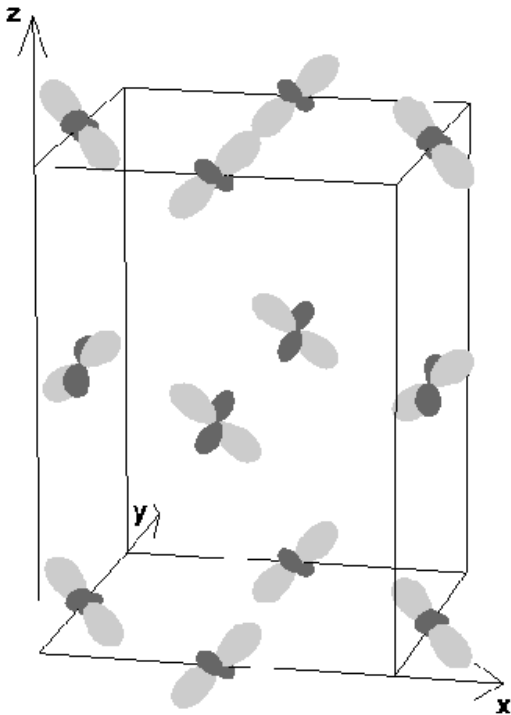


FIG. 2: The orbital order of the Ti ions in YTiO_3 .

moment, $\langle r^2 \rangle$, and the fourth moment, $\langle r^4 \rangle$, of the effective ionic radius of the Ti^{3+} -ion. We have used the values $\langle r^2 \rangle = 0.530 \text{ \AA}^2$ and $\langle r^4 \rangle = 0.554 \text{ \AA}^4$ [17]. The results of the crystal-field calculation, which are listed in Table II, exhibit a t_{2g} splitting scheme where a non-degenerate ground state is clearly separated from the excited states. This ground state orbital, which gives rise to orbital ordering, is given by the first line in Table II and depicted in Fig. 2. It agrees very well with data obtained from nuclear magnetic resonance (NMR) and polarized neutron diffraction experiments [12, 13].

B. The Hamiltonian

We next construct the microscopic Hamiltonian pertaining to the Ti ions, from which we obtain perturbatively the superexchange spin couplings. The calcula-

tion is carried out for a two-site cluster, consisting of two nearest-neighbor Ti ions, denoted by m and n .

The unperturbed part of the Hamiltonian contains the static crystal field, H_{mn}^{cf} , and the intra-ionic Coulomb correlations of a doubly occupied d shell, H_{mn}^{c} ,

$$H_{mn}^0 = H_{mn}^{\text{cf}} + H_{mn}^{\text{c}}. \quad (2)$$

The perturbation calculation carried out below involves two sectors, which together span the Hilbert space of the cluster: A Ti^{3+} sector, in which both Ti ions are trivalent, and a Ti^{2+} sector, where one of the Ti ions is divalent (two d electrons on the same site) and the other is tetravalent (an empty d shell). The ground state of H_{mn}^0 belongs to the Ti^{3+} sector, where both Ti ions are in the one-particle ground state of H_{mn}^{cf} (modulo spin up or down on each site), leading to a four-fold degeneracy of the ground state of the cluster. The spectrum of H_{mn}^0 is found by applying H_{mn}^{cf} on the Ti^{3+} sector, and both H_{mn}^{cf} and H_{mn}^{c} on the Ti^{2+} sector. H_{mn}^{c} is parametrized in terms of the Slater integrals F^2 and F^4 [18], and the effective Ti-Ti charge-transfer energy U_{eff} . This energy is the difference between the four-fold degenerate ground state of the cluster (which is the lowest level of the Ti^{3+} sector) and the lowest level of the Ti^{2+} sector (where H_{mn}^{cf} and H_{mn}^{c} are diagonalized simultaneously). We use $F^2 = 8F^4/5 = 8.3 \text{ eV}$ from an atomic Hartree-Fock calculation [19], and $U_{\text{eff}} = 3.5 \text{ eV}$ from the analysis of the photoemission spectra and first-principles calculations [20]. We note that the charge-transfer energy U_{eff} might have a considerable uncertainty, and in particular may be lower than 3.5 eV. For example, there is a strong resonance in Raman spectroscopy [21] at a laser frequency of 2.54 eV. Since experiment indicates that the resonance is mainly caused by processes involving two Ti sites, it may well be that it yields a lower value for U_{eff} . Further first-principles calculations and a comparison with optical-conductivity data are required in order to determine more precisely U_{eff} .

The perturbation part of the Hamiltonian, V_{mn} , consists of an effective Ti-Ti tunnelling term, H_{mn}^{tun} , and the on-site spin-orbit interaction, H_{mn}^{so} ,

$$V_{mn} = H_{mn}^{\text{tun}} + H_{mn}^{\text{so}}. \quad (3)$$

The tunnelling Hamiltonian is given in terms of an effective hopping matrix, t_{mn} , between the m and the n Ti ions,

$$H_{mn}^{\text{tun}} = \sum_{ij} \sum_{\sigma} t_{mn}^{ij} d_{mi\sigma}^{\dagger} d_{nj\sigma} + \text{H. c.}, \quad (4)$$

where $d_{mi\sigma}^{\dagger}$ ($d_{mi\sigma}$) creates (destroys) an electron with spin σ in the i -th eigen-orbital of H_{mn}^{cf} at site number m (see Table II). The spin-orbit coupling is given by

$$H_{mn}^{\text{so}} = \lambda \sum_{k=m,n} \mathbf{l}_k \cdot \mathbf{s}_k, \quad (5)$$

where \mathbf{l}_k denotes the angular momentum operator of the Ti ion at the k site, \mathbf{s}_k is its spin operator, and λ is the spin-orbit coupling strength. We use $\lambda = 18$ meV [22].

The dominant hopping process between two nearest-neighbor Ti ions is mediated via the oxygen ion which is nearest to both of them. Let $t_m^{i\alpha}$ be the hopping matrix element of an electron in the p orbital α on the oxygen ion into the i state of the Ti ion located at m . The effective hopping between the Ti ions is then given by

$$t_{mn}^{ij} = -\frac{1}{\Delta_{\text{eff}}} \sum_{\alpha} t_m^{i\alpha} t_n^{j\alpha} = t_{nm}^{ji}. \quad (6)$$

Here, Δ_{eff} is the charge-transfer energy, which is required to put an electron from an O ion on a Ti ion, and α denotes one of the three p orbitals on the oxygen (in orthorhombic coordinates),

$$|x\rangle, |y\rangle, |z\rangle. \quad (7)$$

(Modifications of this basis due to the crystal field are ignored, since the crystal field splitting is expected to be small compared to the Ti-O charge-transfer energy.)

Using the structural data from Table I, together with elementary geometric considerations, the Ti-O hopping matrix elements can be expressed in terms of the Slater-Koster parameters $V_{pd\sigma}$ and $V_{pd\pi}$ [23]. We use the values $V_{pd\sigma} = -2.3$ eV, $V_{pd\pi} = 1.1$ eV, and $\Delta_{\text{eff}} = 5.5$ eV [20], in conjunction with Eq. (6) to compute the effective hopping matrices pertaining to the unit cell. The results are listed in Table III, which also gives the symmetry properties of the hopping matrices between different Ti-Ti bonds. The four Ti sites of the unit cell form twelve nearest-neighbor Ti-Ti bonds which are inequivalent, i. e., they do not evolve from each other by Bravais translations. These bonds connect the ten Ti ions indicated in Fig. 1. By the symmetry operations of the space group $Pbnm$, the eight effective hopping matrices between Ti ions belonging to the same ab plane and the four matrices for Ti-Ti bonds along the c direction, respectively, can be expressed by a single matrix each. For example, all twelve hopping matrices are given by the two matrices for the Ti-Ti bonds $mn = 12$ (planar) and $mn = 13$ (inter-planar), respectively.

C. The Ti-O hybridization

Our model does not include the covalent contribution to the crystal field, arising from hybridization between the Ti- $3d$ and O- $2p$ states. This mechanism mixes excited states of the static crystal-field into the Ti^{3+} ground state, i. e., there is an admixture of Ti^{2+} states accompanied by an admixture of holes on the oxygen sites.

Following Refs. [20] and [24], we may estimate the effect of the pd hybridization. When that hybridization is absent, the effective parameter U_{eff} defines the energy difference between the ground state of the Ti^{3+}

TABLE III: The effective Ti-Ti hopping matrices for the d eigen-orbitals of the crystal field from Table II; values are given in eV. The rows and the columns are ordered beginning with the ground state of the crystal field (index 0), continuing with the first excited state (index 1), etc. The matrix t_{13} is symmetric because of a mirror plane, see Ref. [9].

Planar				
$t_{12} = t_{16}^t = t_{25} = t_{65}^t = t_{34} = t_{38}^t = t_{47} = t_{87}^t$				
=	$\begin{bmatrix} -0.062 & -0.206 & 0.033 & -0.026 & -0.012 \\ 0.007 & -0.015 & 0.006 & -0.086 & 0.114 \\ 0.130 & -0.077 & -0.125 & 0.149 & -0.203 \\ -0.202 & 0.030 & 0.092 & 0.453 & -0.632 \\ -0.036 & 0.008 & 0.024 & 0.031 & -0.044 \end{bmatrix}$			
Inter-planar				
$t_{13} = t_{24} = t_{39} = t_{410}$				
=	$\begin{bmatrix} 0.086 & -0.009 & 0.101 & -0.024 & -0.085 \\ -0.009 & 0.160 & 0.043 & 0.126 & 0.227 \\ 0.101 & 0.043 & 0.119 & -0.048 & -0.159 \\ -0.024 & 0.126 & -0.048 & -0.107 & -0.263 \\ -0.085 & 0.227 & -0.159 & -0.263 & -0.607 \end{bmatrix}$			

sector and the lowest state of the Ti^{2+} sector in a two-site cluster consisting of two Ti ions. When the pd hybridization is present, these two types of d states correspond to two bands, from which two pd hybridized bands evolve according to the covalent crystal field. These hybridized bands have, in general, significant dispersion: Their peak-to-peak separation is given by the band gap $E_{\text{gap}}=1.8$ eV [20], and the distance between the band edges is given by the optical gap $E_{\text{opt}}=1.0$ eV [24], which is experimentally observed as the Mott gap. The mean bandwidth between the two pd hybridized bands is then $W = E_{\text{gap}} - E_{\text{opt}} = 0.8$ eV. These bands are not as dispersive as in the case of LaTiO_3 , where the mean bandwidth is $W = 1.4$ eV [25].

Nevertheless, given this dispersion of the bands one may wonder whether a localized picture is appropriate, even approximately, for the YTiO_3 system. In order to study this point, we have analyzed the covalent crystal field of a cluster consisting of a single Ti ion, and the six oxygen ions predominantly hybridized with it (the calculation has been carried out for Ti number 1 in Fig. 1). This is accomplished by diagonalizing the Hamiltonian

$$H_{pd} = H^{\text{cf}} + H^c + H_{pd}^{\text{tun}}, \quad (8)$$

for a TiO_6 -cluster. Here H^{cf} describes the static crystal field, H^c is the Coulomb interaction, and H_{pd}^{tun} is the pd -tunnelling,

$$H_{pd}^{\text{tun}} = \sum_{n\alpha\sigma} \tilde{t}_{1n}^{i\alpha} d_{1i\sigma}^\dagger p_{n\alpha\sigma} + \text{H. c.}, \quad (9)$$

where $p_{n\alpha\sigma}$ destroys an electron on the n -th oxygen site with spin σ in the α -orbital, given in Eq. (7). As in

TABLE IV: The combined static and covalent crystal field for Ti^{3+} (site 1): Spectrum and eigenstates in the orthorhombic basis for the d basis, see Eq. (1).

-0.673 eV	(0.187, -0.340, -0.438, 0.583, -0.564)
-0.519 eV	(-0.028, -0.350, 0.573, 0.622, 0.402)
-0.409 eV	(0.459, 0.274, 0.634, -0.050, -0.557)
0.737 eV	(0.751, 0.342, -0.280, 0.188, 0.453)
0.865 eV	(-0.435, 0.755, -0.036, 0.485, -0.072)

the calculation of the Ti-Ti hopping amplitudes, the pd hopping amplitudes, \tilde{t}_{1n}^α , are expressed in terms of the Slater-Koster parameters $V_{pd\sigma}$ and $V_{pd\pi}$, using the structural data of Ref. [15].

The entire space of the basis states of the TiO_6 -cluster consists of a Ti^{3+} sector where the p orbitals are all occupied, and a Ti^{2+} sector where there is a hole in one of the p orbitals. The eigenstates of the Hamiltonian (8) have the form

$$|\psi\rangle = \sqrt{2-n_d}|d^1\rangle + \sqrt{n_d-1}|d^2\rangle, \quad (10)$$

where n_d is the occupation number of the Ti- d shell ($1 \leq n_d \leq 2$), $|d^1\rangle$ is a state with a single electron in the d shell and fully occupied p shells on the surrounding oxygen ions, and $|d^2\rangle$ is a state with two electrons in the d shell and a hole in the p shell of one of the oxygen ions. We find that in the ground state $n_d = 1.330$, i. e., there is a p hole on one of the neighboring oxygens with probability of 33.0 %.

This calculation allows for the analysis of the eigenstates of the combined static and covalent crystal fields. Projecting the five lowest eigenstates onto the Ti^{3+} sector (which corresponds to the states $|d^1\rangle$), gives to a very good approximation the same eigenstates as for the static crystal field alone, as can be seen by comparing Table IV with Table II. This finding explains why, despite the admixture of Ti^{2+} states $|d^2\rangle$, the agreement with the experiments of Refs. [12] and [13] remains perfect. Indeed, these experiments measure the Ti^{3+} part, $|d^1\rangle$, of the combined static and covalent crystal field, and apparently are not sensitive to the Ti^{2+} admixture $|d^2\rangle$. Table IV also shows that the t_{2g} splitting remains almost the same as in the absence of the covalent contribution, whereas the distance between the t_{2g} and e_g energies is enhanced.

We now discuss the crystal-field gap and the t_{2g} splitting scheme as obtained from our calculation and from an alternative calculation [26], in relation with an analysis of the optical conductivity [26] and Raman data [21]. Our static crystal-field calculation yields a non-degenerate orbital ground state separated by ≈ 0.15 eV from the first excited state and a second excited state separated by ≈ 0.13 eV from the first excited one (see Table II). This t_{2g} splitting scheme results from the orthorhombic distortion of the crystal and from the distortion of the oxygen

octahedra. We have estimated that the covalent crystal field reduces the gap between the first and the second excited states (to about 0.11 eV according to Table IV), while the gap between the ground state and the first excited state remains practically the same. A more precise calculation of the covalent crystal field [26], which takes into account two additional effects, the pp hybridization and the Ti^{1+} admixture [27], gives ≈ 0.19 eV for the gap between the ground state and the first excited state and ≈ 0.14 eV for the gap between the first and the second excited states (the Ti^{1+} admixture means that there is also an admixture of d^3 states to the ground state). This result is in better agreement with the data of optical conductivity [26] and Raman spectroscopy [21], which show that the first orbital excitation is centered around 0.2–0.25 eV.

Since it is extremely complicated to include in the magnetic superexchange calculation the hopping between the pd hybridized states, our calculations below contain only the hopping between the Ti^{3+} states. The results listed in Table IV, which show that the projections of the eigenstates of the combined static and covalent crystal fields onto the Ti^{3+} sector are almost the same as in the static-only case, ensure that the Ti^{3+} ground states we use are an appropriate starting point for the superexchange calculation.

D. The magnetic moment

The calculation of the magnetic structure detailed below yields the directions of the magnetic moments in the ground state, but does not determine the magnitude of the moment. However, one can estimate that magnitude by diagonalizing together H_{mn}^{cf} and H_{mn}^{so} for a single Ti^{3+} ion. The eigenstates of this combined Hamiltonian are symmetric or antisymmetric with respect to time-reversal, leading to five Kramers doublets for the single Ti^{3+} ion. We use those doublets to find the expectation values of the angular momentum. By choosing the largest possible polarization of the magnetic moment along the z axis (that direction is the leading one of the observed moment [2]) out of all the linear combinations of the ground-state doublet, we find $\langle l_k^z + 2s_k^z \rangle \mu_B = 0.91 \mu_B$. This partially explains the reduction of the observed ordered moment as compared to $1 \mu_B$.

The Ti-O hybridization hardly affects the magnetic moment. For the parameters used here, the admixture of spin 0 and spin 1 Ti^{2+} states into the ground state of the covalent crystal field reduces the ordered moment by only ≈ 0.1 %.

III. THE SUPEREXCHANGE COUPLINGS

Our aim is to obtain from the full Hamiltonian, $H_{mn} = H_{mn}^0 + V_{mn}$, an effective spin Hamiltonian, h_{mn} , which

acts within the Hilbert space of the four-fold degenerate ground state of the unperturbed Hamiltonian H_{mn}^0 .

Since the Hamiltonian is invariant under time-reversal, there are no single-ion terms, and consequently the effective spin Hamiltonian, to second-order in the spin variables, takes the form

$$h_{mn} = \mathbf{S}_m \cdot A_{mn} \cdot \mathbf{S}_n, \quad (11)$$

where A_{mn} ($= A_{nm}^t$) is the 3×3 superexchange matrix. This matrix may be decomposed into a symmetric part and an antisymmetric one. The three components of the latter constitute the Moriya vector \mathbf{D}_{mn} ($= -\mathbf{D}_{nm}$). Extracting further the isotropic part of A_{mn} , i.e., the Heisenberg coupling J_{mn} , the effective spin Hamiltonian is cast into the form

$$h_{mn} = J_{mn} \mathbf{S}_m \cdot \mathbf{S}_n + \mathbf{D}_{mn} \cdot (\mathbf{S}_m \times \mathbf{S}_n) + \mathbf{S}_m \cdot A_{mn}^s \cdot \mathbf{S}_n. \quad (12)$$

Here, A_{mn}^s represents the symmetric anisotropy. Due to the space-group symmetries, all three types of magnetic couplings belonging to the eight planar Ti-Ti bonds may be obtained from those of a single bond, and so is the case for the four inter-planar bonds, see Ref. [9].

The various magnetic couplings appearing in Eq. (12) are obtained by perturbation theory to leading order in V_{mn} , namely, to second order in the hopping t_{mn} and to first and second order in the spin-orbit coupling (scaled by λ). The formal expressions of the perturbation expansion are documented in Ref. [9]. The Heisenberg isotropic exchange [the first term in Eq. (12)] is independent of λ . A systematic description of the magnetic anisotropies due to the spin-orbit interaction requires both the first and the second order processes in λ [29]. The technical reason being that the expectation value of the cross product in the second term of Eq. (12) is, in fact, also of order λ , so that altogether the Dzyaloshinskii-Moriya interaction contributes to the exchange energies in at least second order in the spin-orbit coupling. We neglect terms in which there appear two Ti^{2+} intermediate states in the perturbation expansions. These are smaller than the ones we keep, by an additional factor of $\simeq \Delta_{\text{cf}}/U_{\text{eff}} = 0.043$, where $\Delta_{\text{cf}} = 0.150 \text{ eV}$ is the gap between the ground state of the single-particle crystal field and the first excited state, see Table II. The detailed calculation of the various terms is lengthy, albeit straight-forward. More details are given in Ref. [9]. The values we obtain, using the parameters cited above, are listed in Table V.

As is seen from Table V, the value we find for the in-plane Heisenberg coupling, J_{12} , roughly agrees with the experimental one, $\approx -3 \text{ meV}$ [3]. However, the calculated inter-plane coupling, J_{13} , is *positive*, in contradiction with experiment [3] (which yields for that coupling $\approx -3 \text{ meV}$, too). Generally speaking, there are antiferromagnetic and ferromagnetic contributions to the isotropic Heisenberg couplings. The former arise when the intermediate Ti^{2+} states of the perturbation expansion are singlets, and the latter when they are triplets. Separating these competing contributions, we find $J_{12}^s = 21.481$

TABLE V: The calculated single-bond spin couplings (in meV). The Moriya vectors are given including the corrections \mathbf{D}'_{mn} , which are of order λ^2 . The symmetric anisotropies are given as $\mathbf{A}_{mn}^d = (A_{mn}^{xx}, A_{mn}^{yy}, A_{mn}^{zz})$ and $\mathbf{A}_{mn}^{\text{od}} = (A_{mn}^{yz}, A_{mn}^{xz}, A_{mn}^{xy})$ for the diagonal and off-diagonal entries, respectively.

Heisenberg couplings	
$J_{12} = -3.870, J_{13} = 2.772$	
Moriya vectors	
$\mathbf{D}_{12} = (1.776, -0.938, -0.325), \mathbf{D}_{13} = (-0.671, 0.189, 0)$	
Symmetric anisotropies	
$\mathbf{A}_{12}^d = (0.175, -0.011, -0.160), \mathbf{A}_{13}^d = (-0.145, -0.024, 0.010),$ $\mathbf{A}_{12}^{\text{od}} = (0.044, -0.131, -0.313), \mathbf{A}_{13}^{\text{od}} = (0, 0, -0.153)$	

meV, $J_{12}^t = -25.351 \text{ meV}$, $J_{13}^s = 12.008 \text{ meV}$, and $J_{13}^t = -9.237 \text{ meV}$, namely, the antiferromagnetic and the ferromagnetic contributions are roughly the same. It is worth noting that in the case of LaTiO_3 [9], the contribution of the singlets dominated the one of the triplets, and indeed our calculation of that compound has yielded reliable values. Unfortunately, in the case of YTiO_3 the balance between these competing contributions is too sensitive to be resolved by our model approximations. This delicate balance in the case of YTiO_3 is also reflected in the overall rather small value of the total isotropic coupling, $\approx -3 \text{ meV}$, (whereas it is 15.5 meV in the case of LaTiO_3). This value is also very sensitive to the parameters used. For example, taking $U_{\text{eff}} \approx 1.6 \text{ eV}$ would have changed the sign of J_{13} . In contrast, a sign change in the case of LaTiO_3 requires the considerably lower value of $U_{\text{eff}} \approx 0.6 \text{ eV}$. We discuss in Sec. VI various difficulties encountered in obtaining realistic values for the Heisenberg couplings of YTiO_3 which have been previously reported in the literature.

Had we used the values listed in Table V, we would have obtained a predominant A-type antiferromagnetic order for YTiO_3 , which sharply contradicts the experiment [3]. However, the fact that our values for the leading (isotropic) superexchange couplings do not agree with experiment does not necessarily mean that the anisotropic ones are not reliable. In the case of the cuprates, for example, it has been found (by comparing with exact diagonalizations) that while the isotropic couplings calculated by perturbation theory were inaccurate, the anisotropic ones were accurate enough [11]. Since the latter determine the directions of the spins in the classical ground state and the spin-wave gaps, a way to test our anisotropic superexchange couplings is to examine those properties. In order to do so, we replace in the following the isotropic couplings by the experimentally-deduced ones, $J_{12} = J_{13} = -2.75 \text{ meV}$ [3], while using for the anisotropic couplings the values given in Table V.

IV. THE MAGNETIC STRUCTURE

The single-bond spin Hamiltonian, Eq. (12), is the basis for the magnetic Hamiltonian, from which the magnetic order of the classical ground state follows. To construct the latter, the entire Ti-lattice is decomposed into four sublattices. The four sublattices are enumerated according to the numbers of the four Ti ions per unit cell shown in Fig. 1 (sublattice $i = 1$ corresponds to Ti ion 1 and its Bravais translations, etc.). Assigning a fixed magnetization (per site) to all the spins within each sublattice, \mathbf{M}_i , one sums over all bonds which couple the four sublattices, to obtain the *macroscopic* magnetic Hamiltonian in the form

$$H_M = \sum_{ij} [I_{ij} \mathbf{M}_i \cdot \mathbf{M}_j + \mathbf{D}_{ij}^D \cdot (\mathbf{M}_i \times \mathbf{M}_j) + \mathbf{M}_i \cdot \Gamma_{ij} \cdot \mathbf{M}_j], \quad (13)$$

where ij runs over the sublattice pairs 12, 13, 24, and 34 of Fig. 1. This summation procedure gives rise to the macroscopic magnetic couplings: I_{ij} is the macroscopic isotropic coupling, \mathbf{D}_{ij}^D are the Dzyaloshinskii vectors which are the macroscopic antisymmetric anisotropies, and Γ_{ij} are the macroscopic symmetric anisotropy tensors. The relations between those macroscopic couplings and the microscopic single-bond couplings and the inter-relations among the macroscopic couplings, dictated by the symmetries of the space-group, are discussed in Ref. [9].

We now minimize H_M , and find the various sublattice magnetizations. We assume that all four vectors \mathbf{M}_i have the same magnitude, M , but differ in their directions. Since Eq. (13) is quadratic in M , the minimization will only yield the directions of these vectors, and not the value of M . To simplify the procedure we use group theory. According to the space group $Pbnm$ symmetries, there are four possibilities for the symmetry of sublattice magnetizations of the classical ground state, as listed in Ref. [30]. Having checked each of them, we have concluded that only one of these possibilities has the lowest energy. We then find that the classical magnetic ground state has the following structure: The x components of the magnetizations order antiferromagnetically, in a G-type structure (where the four sublattices actually reduce to two). The y components order antiferromagnetically as well, but in an A-type structure. Finally, the z components of the magnetizations order ferromagnetically.

This structure agrees with experiment [3]. This is a non-trivial result caused by the anisotropic spin couplings. Given only the ferromagnetic Heisenberg couplings, the ferromagnetic moment could also be oriented along the x or the y axis, see Ref. [30].

The magnetic structure can be specified by expressing the four magnetizations in terms of two canting angles, φ and ϑ , see Tables VI and VII. The angle ϑ , measured with respect to the z axis, is proportional to the spin-orbit parameter λ (as found by varying this parameter), while the angle φ is almost *independent* of it. Indeed,

TABLE VI: The structure of the magnetic order in YTiO₃, characterized in terms of the sublattice magnetizations \mathbf{M}_i in the classical ground state (normalized to the value M), which are expressed by the canting angles φ and ϑ .

x components: G-type
$-M_1^x = M_2^x = M_3^x = -M_4^x = M \cos \varphi \sin \vartheta$
y components: A-type
$-M_1^y = -M_2^y = M_3^y = M_4^y = M \sin \varphi \sin \vartheta$
z components: ferromagnetic
$M_1^z = M_2^z = M_3^z = M_4^z = M \cos \vartheta$

one may verify that for an infinitesimally small λ , there is just a ferromagnetic order along the z axis. As λ increases, so does ϑ , causing an increasing canting of the magnetizations. However, the projection of the magnetic moment onto the xy planes remains almost perpendicular to the rotation axis of the magnetization, and hence φ is practically unaffected by the value of λ . Interestingly enough, the magnetic structure of LaTiO₃ can also be described in terms of such canting angles. However, in that case both φ and ϑ (the latter measured with respect to the xy planes) are proportional to λ [9], leading to a (mainly) G-type order along the x direction which would have occurred even for an infinitesimally small λ .

It is worth noting that using naively the procedure outlined above to obtain the energy of the classical magnetic ground-state might yield non-systematic contributions up to fourth order in the spin-orbit coupling λ [9, 29]. To exemplify this point, we consider the expectation value of H_M , expressed in terms of the canting angles φ and ϑ ,

$$\begin{aligned}
\langle H_M \rangle = & [\lambda^0 :] \quad 2(I_{12} + I_{13}) \cos^2 \vartheta \\
& [\lambda^2 :] - 2(I_{12} + I_{13}) \cos^2 \varphi \sin^2 \vartheta + 2(I_{12} - I_{13}) \sin^2 \varphi \sin^2 \vartheta \\
& \quad + 4(D_{12}^{Dy} + D_{13}^{Dy}) \cos \varphi \cos \vartheta \sin \vartheta - 4D_{13}^{Dx} \sin \varphi \cos \vartheta \sin \vartheta + 2(\Gamma_{12}^{zz} + \Gamma_{13}^{zz}) \cos^2 \vartheta \\
& [\lambda^3 :] + 4D_{12}^{Dz} \cos \varphi \sin \varphi \sin^2 \vartheta - 2\Gamma_{12}^{yz} \sin \varphi \cos \vartheta \sin \vartheta \\
& [\lambda^4 :] - 2(\Gamma_{12}^{xx} + \Gamma_{13}^{xx}) \cos^2 \varphi \sin^2 \vartheta + 2(\Gamma_{12}^{yy} - \Gamma_{13}^{yy}) \sin^2 \varphi \sin^2 \vartheta - 4\Gamma_{13}^{xy} \cos \varphi \sin \varphi \sin^2 \vartheta.
\end{aligned} \tag{14}$$

TABLE VII: The macroscopic magnetic couplings in meV, the resulting canting angles of the magnetizations in the classical ground state, and the resulting values of the ordered moments (normalized to the value M). Three coefficients of the macroscopic symmetric anisotropies are taken into account (see text).

Isotropic couplings
$I_{12} = -2.750, I_{13} = -1.375$
Dzyaloshinskii vectors
$\mathbf{D}_{12}^D = (0, -0.938, -0.367), \mathbf{D}_{13}^D = (-0.335, 0.094, 0)$
Macroscopic symmetric anisotropies
$\Gamma_{12}^{zz} = -0.160, \Gamma_{13}^{zz} = 0.005, \Gamma_{12}^{yz} = 0.044$
Canting angles
$\varphi = -44.17^\circ, \vartheta = 7.55^\circ$
Ordered moments
$\mathbf{M} = (\pm 0.094, \pm 0.092, 0.991) M$

We take the contributions up to the order λ^3 into account, i. e., we *exclude* from the calculation of the classical ground state the coefficients $\Gamma_{12}^{xx}, \Gamma_{13}^{xx}, \Gamma_{12}^{yy}, \Gamma_{13}^{yy}, \Gamma_{13}^{xy}$, and the λ^2 correction of D_{12}^{Dz} . This procedure yields the *macroscopic* magnetic couplings listed in Table VII. Using these couplings we have calculated the canting angles φ and ϑ , and the ordered magnetic moments. These results are also listed in Table VII.

In order to compare our magnetic structure with the one found experimentally, we normalize the moments to $1 \mu_B$. Then, according to Ref. [3], experiment gives $\mathbf{M} = (\pm 0.149, \pm 0.085, 0.985) \mu_B$, with relative errors of 15 % for the G-type moment, 25 % for the A-type moment, and 2 % for the ferromagnetic moment. The calculated values are within a single error bar except for the G-type moment for which we obtain a value which is 37 % lower than the experimental one (i. e., within the 3σ range of the measurement). Thus, the calculated magnetic structure is in reasonable agreement with experiment.

V. THE SPIN-WAVE SPECTRUM

A. The spin-wave Hamiltonian

The calculation of the spin-wave dispersion is carried out analogously to the case of LaTiO₃ [9], since all symmetries are the same for both YTiO₃ and LaTiO₃. As in the calculation of the classical magnetic ground state, we combine the experimental Heisenberg couplings $J_{12} = J_{13} = -2.75$ meV [3] with our calculated anisotropic couplings which contribute systematically to the classical ground-state energy [see Eq. (14) and the following discussion].

Since the classical magnetic ground state is characterized by four sublattices, we will obtain four branches in the spin-wave dispersion. The first step in the standard calculation of spin-wave dispersions is the rotation of the local coordinates at each sublattice, i , such that the new z axis will point in the direction of the corresponding sublattice ground-state magnetization, \mathbf{M}_i . This rotation still leaves the freedom to choose the new local x and y axes, i. e., to rotate the new coordinate system around its z axis. Denoting the new local coordinate system by x'_i, y'_i and z'_i ($i = 1, 2, 3, 4$), we find that the convenient choice for our purpose is

$$\begin{aligned}
\hat{z}'_i &= \frac{\mathbf{M}_i}{M}, \quad \hat{y}'_i = \frac{\mathbf{M}_i \times \hat{x}}{m_i}, \quad \hat{x}'_i = \hat{y}'_i \times \hat{z}'_i, \quad M = |\mathbf{M}_i|, \\
m_i &= \sqrt{(M_i^y)^2 + (M_i^z)^2}.
\end{aligned} \tag{15}$$

In the rotated coordinate system the spin Hamiltonian, comprising all three types of magnetic couplings, takes the form

$$h = \sum_{\langle mn \rangle} \mathbf{S}'_m \cdot A'_{mn} \cdot \mathbf{S}'_n, \tag{16}$$

where the primes denote the rotated quantities. In particular, A'_{mn} is the 3×3 superexchange matrix in rotated coordinates.

Since we consider only the Ti ions, it is convenient to use a coordinate system in which the Ti ions occupy the sites of a simple cubic lattice, of unit lattice constant (this picture is the appropriate one for comparing with the experimental spin-wave data [3], as discussed in the

next subsection). It is also convenient to use a coordinate system in which nearest-neighbor Ti ions are located along the axes (namely, to rotate the orthorhombic coordinates by -45° around the z axis, see Fig. 1). Accord-

ingly, our magnetic unit cell is spanned by the vectors $(1, 1, 0)$, $(1, -1, 0)$, and $(0, 0, 2)$, and the corresponding magnetic Brillouin zone (MBZ) is defined by

$$|q_x + q_y| \leq \pi, \quad |q_z| \leq \frac{\pi}{2}. \quad (17)$$

The resulting spin-wave dispersion (for more details of the derivation, see Ref. [9]) consists of four branches,

$$\begin{aligned} \Omega_1^2(\mathbf{q}) &= (C_1 + C_2^\perp \cos q_z)^2 - |C_3^\perp|^2 \cos^2 q_z + |C_2^\parallel|^2 (\cos q_x + \cos q_y)^2 - |C_3^\parallel \cos q_x + C_3^{\parallel*} \cos q_y|^2 \\ &\quad - (\cos q_x + \cos q_y) W(-\cos q_z), \\ \Omega_2^2(\mathbf{q}) &= \Omega_1^2(\mathbf{q} + \mathbf{Q}), \quad \text{with } \mathbf{Q} = (0, 0, \pi), \\ \Omega_3^2(\mathbf{q}) &= \Omega_1^2(\mathbf{q} + \mathbf{Q}'), \quad \text{with } \mathbf{Q}' = (\pi, \pi, 0), \\ \Omega_4^2(\mathbf{q}) &= \Omega_1^2(\mathbf{q} + \mathbf{Q}''), \quad \text{with } \mathbf{Q}'' = \mathbf{Q} + \mathbf{Q}' = (\pi, \pi, \pi), \end{aligned} \quad (18)$$

where

$$\begin{aligned} W^2(\cos q_z) &= 4 \left[(C_1 - C_2^\perp \cos q_z)^2 - |C_3^\perp|^2 \cos^2 q_z \right] \left[|C_2^\parallel|^2 - \left(\frac{C_3^\parallel + C_3^{\parallel*}}{2} \right)^2 \right] \\ &\quad + \left[(C_3^{\perp*} C_2^\parallel + C_3^\perp C_2^{\parallel*}) \cos q_z + (C_1 - C_2^\perp \cos q_z) (C_3^\parallel + C_3^{\parallel*}) \right]^2. \end{aligned} \quad (19)$$

Each of the spin-wave branches has tetragonal symmetry, i.e., $\Omega_i(q_x, q_y, q_z) = \Omega_i(q_y, q_x, q_z) = \Omega_i(-q_x, q_y, q_z) = \Omega_i(q_x, -q_y, q_z) = \Omega_i(q_x, q_y, -q_z)$. The coefficients in Eqs. (18) and (19) are linear combinations of the coefficients $C_{mn}(\ell)$,

$$C_1 = 2C_{13}(1) + 4C_{12}(1) = C_1^*, \quad C_2^\perp = 2C_{13}(2) = C_2^{\perp*}, \quad C_2^\parallel = 2C_{12}(2), \quad C_3^\perp = 2C_{13}(3), \quad C_3^\parallel = 2C_{12}(3). \quad (20)$$

These are given by combinations of the superexchange matrix elements $(A'_{mn})^{\alpha\beta}$,

$$\begin{aligned} C_{mn}(1) &= -\frac{1}{2} (A'_{mn})^{zz}, \\ C_{mn}(2) &= \frac{1}{4} [(A'_{mn})^{xx} + (A'_{mn})^{yy} + i((A'_{mn})^{yx} - (A'_{mn})^{xy})], \\ C_{mn}(3) &= \frac{1}{4} [(A'_{mn})^{xx} - (A'_{mn})^{yy} + i((A'_{mn})^{yx} + (A'_{mn})^{xy})]. \end{aligned} \quad (21)$$

The explicit expressions are not reproduced here since their expressions are very long.

Equations (18) contain our final result for the spin-wave spectrum of YTiO₃. Evidently, the details of the spectrum can be obtained only numerically: One has to write the spin-wave coefficients, Eqs. (20), in terms of those appearing in Eqs. (21), and express the latter in terms of the original coefficients of the spin Hamiltonian (12). These results are then used in constructing the dispersion.

When the spin-orbit parameter λ is set to zero the coefficients appearing in Eqs. (18) simplify to

$$C_1 = -2J_{12} - J_{13}, \quad C_2^\perp = J_{13}, \quad C_2^\parallel = J_{12}, \quad C_3^\perp = C_3^\parallel = 0, \quad (22)$$

where $J_{12} < 0$ is the in-plane Heisenberg coupling, and $J_{13} < 0$ is the Heisenberg coupling between planes. In

that case

$$\begin{aligned} \Omega_1^2(\mathbf{q}) &= [2J_{12} + J_{13} - J_{12}(\cos q_x + \cos q_y) - J_{13} \cos q_z]^2, \\ \Omega_2^2(\mathbf{q}) &= [2J_{12} + J_{13} - J_{12}(\cos q_x + \cos q_y) + J_{13} \cos q_z]^2, \\ \Omega_3^2(\mathbf{q}) &= [2J_{12} + J_{13} + J_{12}(\cos q_x + \cos q_y) - J_{13} \cos q_z]^2, \\ \Omega_4^2(\mathbf{q}) &= [2J_{12} + J_{13} + J_{12}(\cos q_x + \cos q_y) + J_{13} \cos q_z]^2. \end{aligned} \quad (23)$$

Only $\Omega_1(\mathbf{q})$ vanishes at the zone center and is hence termed the acoustic mode. The other branches have gaps at the zone center: $\Omega_2(\mathbf{0}) = 2|J_{13}|$, $\Omega_3(\mathbf{0}) = 4|J_{12}|$, $\Omega_4(\mathbf{0}) = 4|J_{12}| + 2|J_{13}|$, and are hence termed the optical modes. Indeed, when only the ferromagnetic couplings J_{12} and J_{13} are kept (i.e., for $\lambda = 0$), the magnetic unit cell contains only one Ti ion, corresponding a simple cubic lattice. The Brillouin zone is then four times as large as the Brillouin zone of Eq. (17). By "folding out" the

three optical modes into the larger Brillouin zone, one reproduces the usual gapless dispersion of the pure (ferromagnetic) Heisenberg model. At finite values of the spin-orbit coupling all modes have gaps at the zone center, but the one of Ω_1 is much smaller than those of the other three modes.

B. Numerical results for the spin-wave dispersion

1. The acoustic branch

Using an isotropic ferromagnetic nearest-neighbor Heisenberg coupling $J = -2.75$ meV for all bonds, an

$$\Omega(\mathbf{q}) \simeq \sqrt{|J|[3 - (\cos q_x + \cos q_y + \cos q_z)] + \Delta + A(1 - \cos q_x)} \sqrt{|J|[3 - (\cos q_x + \cos q_y + \cos q_z)] + \Delta + A(1 - \cos q_y)}. \quad (24)$$

The numerically-fitted zone-center gap is extremely small. On the other hand, Ref. [3] reports an upper bound, 0.3 meV, for the gap Δ . We find for the acoustic branch

$$\Delta_1 = \Omega_1(\mathbf{0}) = 0.326 \text{ meV}. \quad (25)$$

This value for the zone-center gap roughly agrees with the upper bound according to Ref. [3]. A more severe discrepancy concerns the anisotropy parameter A . This parameter implies that the diagonal and off-diagonal entries of the symmetric anisotropy tensors are given by

$$\begin{aligned} \mathbf{A}_{12}^d &= \frac{1}{2}(A, A, 0) = (0.4, 0.4, 0) \text{ meV}, \\ \mathbf{A}_{13}^d &= (0, 0, A) = (0, 0, 0.8) \text{ meV}, \\ \mathbf{A}_{12}^{\text{od}} &= \frac{1}{2}(0, 0, -A) = (0, 0, -0.4) \text{ meV}, \\ \mathbf{A}_{13}^{\text{od}} &= (0, 0, 0). \end{aligned} \quad (26)$$

This result is in contrast with our calculated values for the symmetric anisotropy tensors according to Table V. However, as is noted above [see Eq. (14)] and also elsewhere [9], *both antisymmetric as well as symmetric anisotropies contribute to the same order in the spin-orbit parameter to the classical ground-state energy and hence to the spin-wave gap and its dispersion. In other words, it is not possible to express all anisotropies in terms of a single parameter and the zone-center gap, or alternatively, it is not possible to deduce the strength of the Dzyaloshinskii-Moriya interaction directly from the spin-wave dispersion. A proper procedure is to compare the full measured and calculated dispersions. Figures 3 (a)–(c) show such a comparison. The agreement of the calculated acoustic branch with the experimental function of Eq. (24) is satisfying (though it is quantitatively not as good as in case of LaTiO₃). The calculated tetrag-*

onal anisotropy parameter $A = 0.8$ meV (which expresses the symmetric anisotropies which are allowed in a cubic situation), and a zone-center gap $\Delta = 0.093 \frac{A^2}{|J|} = 0.02$ meV, the authors of Ref. [3] have fitted the measured neutron-scattering data numerically onto the dispersion,

onal anisotropy of the acoustic branch is found to be

$$\frac{\Omega_1(0, 0, \frac{\pi}{2})}{\Omega_1(\frac{\pi}{2}, 0, 0)} = 97.74 \%. \quad (27)$$

This value is smaller compared to the one found for LaTiO₃ [9], mainly because in the present case the Heisenberg couplings are taken to be isotropic over the lattice.

2. The optical branches

There is experimental evidence for optical spin-wave branches, though this has not been pointed out explicitly in Ref. [3]. There, a plot of the dispersion along the (0,0,1) direction (in the pseudocubic coordinates also used here) is shown. The plot range includes wave vectors (in our notation) $\mathbf{q} = \pi/2(0, 0, 1)\xi$ with $\xi = 0 \dots 2$. One may note however, that for $\xi > 1$ these wave vectors are located *outside* the (first) MBZ, see Eq. (17). The reason is that $\mathbf{Q} = (0, 0, \pi)$ [as well as $\mathbf{Q}' = (\pi, \pi, 0)$] is a site on the reciprocal lattice of sublattice No. 1 and thus, is equivalent to zero wave vector. Were YTiO₃ a ferromagnet without any spin canting, then all four magnetic sublattices would have combined to form a single lattice, and \mathbf{Q} , \mathbf{Q}' , and $\mathbf{Q}'' = \mathbf{Q} + \mathbf{Q}'$ would not be sites of the reciprocal lattice. In this hypothetical case the MBZ would be given by $|q_x|, |q_y|, |q_z| \leq \pi$. In the actual case, with the spin canting, the MBZ is four times smaller than that. We prefer to fold back the data from Ref. [3] to this smaller MBZ, i. e., not to consider only the experimental fit function $\Omega(\mathbf{q})$, but also $\Omega(\mathbf{q} + \mathbf{Q})$, $\Omega(\mathbf{q} + \mathbf{Q}')$, and $\Omega(\mathbf{q} + \mathbf{Q}'')$. We have plotted Figs. 3 (a)–(c) using the back-folded MBZ. The experimental curves which are folded back into the MBZ of the canted ferro-

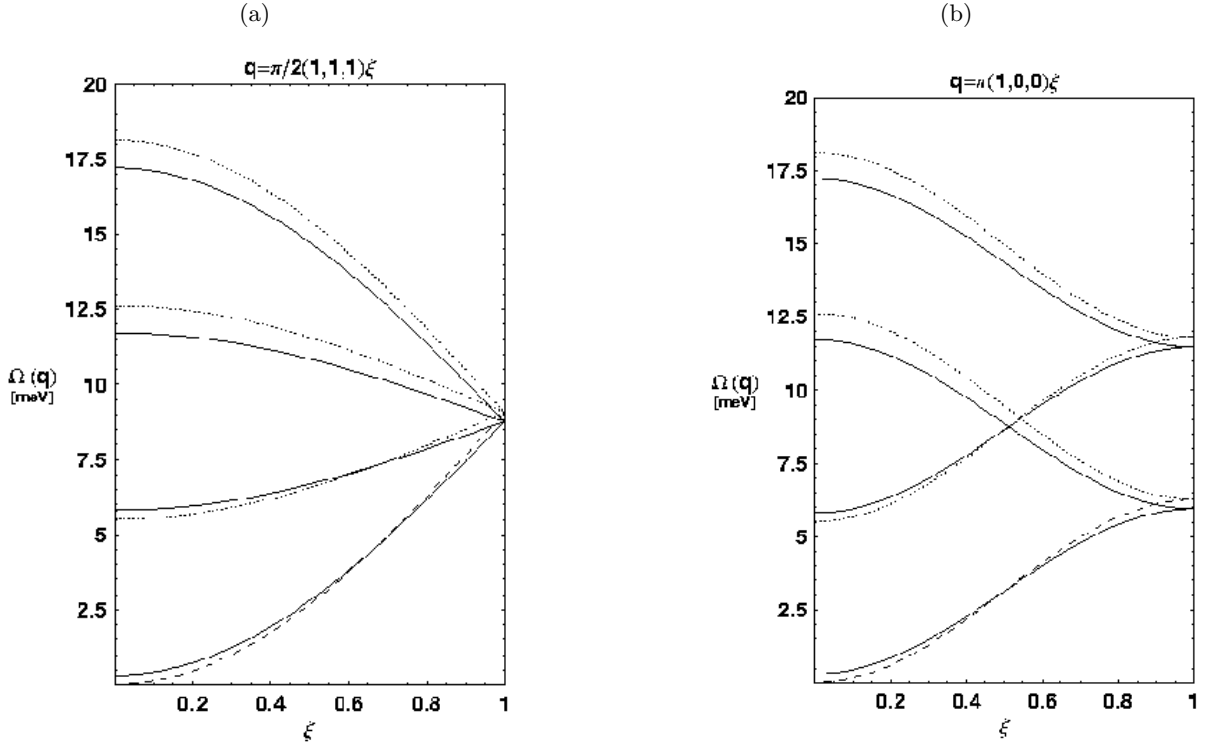


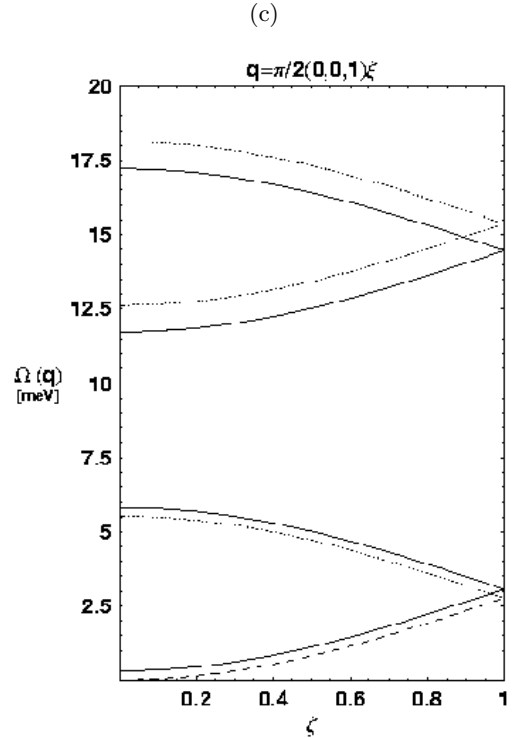
FIG. 3: The spin-wave dispersion along selected directions in the magnetic Brillouin zone. Panels (a)–(c) show the four branches $\Omega_i(\mathbf{q})$ of our calculated dispersion (solid curves), the single branch $\Omega(\mathbf{q})$ (dashed curves) which has been fitted onto neutron-scattering experiments, Eq. (24), according to Ref. [3], and three branches, which are obtained from $\Omega(\mathbf{q})$ by folding it back from the MBZ of the uncanted ferromagnet into the smaller MBZ of the canted ferromagnet (dotted curves, see text). (a) The dispersion along the direction $(1,1,1)$; (b) the dispersion along $(1,0,0)$; (c) the dispersion along $(0,0,1)$.

magnet are in a satisfying agreement with our calculated optical branches. In fact, the signature of the optical spin-wave mode with the largest zone-center gap can be seen in the plots of Ref. [3]. There, it is related to the wave vector \mathbf{Q}'' (which is equivalent to zero wave vector) and has an energy of about 18 meV.

We suggest to re-analyze also the spin-wave data on LaTiO_3 [10], i. e., to fold the experimentally-deduced dispersion $\Omega(\mathbf{q})$ from the MBZ of the antiferromagnet without spin canting back to the MBZ of the canted antiferromagnet (which is half as large), considering also $\Omega(\mathbf{q} + \mathbf{Q})$. Then one obtains the result that the optical branches which have been calculated in Ref. [9] are consistent with the experimental fit function of Ref. [10] for the dispersion.

In the following, we summarize the properties of the calculated optical branches of YTiO_3 . They have considerable zone-center gaps,

$$\begin{aligned} \Delta_2 = \Omega_2(\mathbf{0}) &= 5.815 \text{ meV}, \quad \Delta_3 = \Omega_3(\mathbf{0}) = 11.721 \text{ meV}, \\ \Delta_4 = \Omega_4(\mathbf{0}) &= 17.214 \text{ meV}. \end{aligned} \quad (28)$$



Two of the calculated optical branches have considerable

tetragonal anisotropies,

$$\begin{aligned} \frac{\Omega_2(0, 0, \frac{\pi}{2})}{\Omega_2(\frac{\pi}{2}, 0, 0)} &= 35.48 \%, & \frac{\Omega_3(0, 0, \frac{\pi}{2})}{\Omega_3(\frac{\pi}{2}, 0, 0)} &= 163.29 \%, \\ \frac{\Omega_4(0, 0, \frac{\pi}{2})}{\Omega_4(\frac{\pi}{2}, 0, 0)} &= 100.77 \%. \end{aligned} \quad (29)$$

As is seen in Figs. 3 (a)–(c), all four spin-wave modes are highly non-degenerate over a wide range of the MBZ. In contrast, in the case of LaTiO₃ we have found [9] that the four modes constitute two pairs of quasi-degenerate branches. The reason for this difference between the two systems is related to the smallness of the angle φ in LaTiO₃ (as opposed to its significant value in the case of YTiO₃, see Table VII). In LaTiO₃ there is a nearly full translational symmetry, leading to the quasi-degeneracy of the modes.

VI. SUMMARY AND DISCUSSION

We have presented a detailed model that aims to describe the orbital and the magnetic orders in YTiO₃. While the orbital order that we have calculated turns out to agree very well with experiment, this is not the case for the magnetic superexchange couplings: To the lowest order in perturbation theory, we find that the approximate isotropic coupling between the *ab* planes is antiferromagnetic, while experiment indicates that it is ferromagnetic. This discrepancy is apparently due to a strong competition between ferromagnetic and antiferromagnetic contributions to that coupling. The approximations we employ are not sensitive enough to resolve successfully this competition. In particular, the neglect of exchange processes which involve double *p* holes in the intermediate states, and of the Ti²⁺ admixture into the ground state caused by the covalent crystal field may be detrimental to the calculation of the isotropic magnetic coupling.

In fact, the titanates are notorious for the difficulties one encounters when trying to microscopically derive their properties. For example, Ref. [4] finds a predominant A-type antiferromagnetic coupling for LaTiO₃ while Ref. [5] predicts a ferromagnetic one, both contradicting the experimentally detected G-type coupling of that material. Our work on that compound [9] has yielded the correct magnetic order, but the application of the same model to YTiO₃ turns out to be not so successful. Similar problems have been reported in other studies of YTiO₃. Reference [6], while deriving ferromagnetic couplings, predicts (in contradiction to the experiment) a strong anisotropy between the intra and the inter-plane couplings, i.e., $J_{12} = -2.0$ meV and $J_{13} = -0.6$ meV. Ref.

[3] finds antiferromagnetic values for both these couplings in a parameter range which is considered to be realistic. Both these papers use models which are different than ours, but they also employ perturbation theory to second order in the Ti–Ti hopping to derive the required superexchange parameters.

It should be emphasized, however, that the starting point of our model, i.e., the crystal field and the orbital ordering it implies do give a faithful description for YTiO₃. The failure of our model in producing correctly the isotropic Heisenberg coupling between the *ab* planes is likely to be related to the use of low order perturbation theory and to subtle inaccuracies in the parameters used. The alternative possibility suggested in Ref. [3] based on orbital fluctuations is, in our opinion, not adequate, since it defies the experimentally-detected orbital order of the ground state.

In view of the above difficulties, and since it is known that perturbation theory may be insufficient for the leading isotropic couplings but may well be reliable for the anisotropic ones, we have combined together the experimentally-deduced isotropic couplings of YTiO₃ with the computed anisotropic ones, to calculate the classical magnetic ground state. The result turns out to be satisfactory, when compared with experiment. Similarly to LaTiO₃, we obtain a G-type moment along the crystallographic *a* axis, an A-type moment along the *b* axis, and a ferromagnetic moment along the *c* axis, the latter being the predominant one. Remarkably, this detailed structure is caused by the anisotropies, and cannot be derived solely on the basis of symmetry arguments.

An even further check of our procedure is provided by the calculation of the spin-wave excitations. We find four dispersions: Three of them have considerable zone-center gaps, 6 meV, 12 meV, and 17 meV, while the fourth one has a very small gap, of the order of 0.3 meV, and is approximately isotropic over the magnetic Brillouin zone. We have demonstrated that all branches have experimental counterparts as can be deduced from neutron-scattering data. Comparing the calculated dispersion with the experimental one, we have found that they are in a plausible agreement.

Acknowledgments

We gratefully acknowledge discussions with M. Braden, M. Grüninger, A. B. Harris, M. W. Haverkort, and A. Komarek. This work was partially supported by the German-Israeli Foundation for Scientific Research and Development (GIF).

[1] M. Mochizuki and M. Imada, *New J. Phys.* **6**, 154 (2004).
 [2] J. D. Garret and J. E. Greedan, *Inorg. Chem.* **20**, 1025

(1981).

[3] C. Ulrich, G. Khaliullin, S. Okamoto, M. Reehuis, A.

- Ivanov, H. He, Y. Taguchi, Y. Tokura, and B. Keimer, Phys. Rev. Lett. **89**, 167202 (2002).
- [4] M. Mochizuki and M. Imada, J. Phys. Soc. Jpn. **70**, 1777 (2001).
- [5] M. Mochizuki, J. Phys. Soc. Jpn. **71**, 2039 (2002).
- [6] I. V. Solovyev, Phys. Rev. B **69**, 134403 (2004).
- [7] S. Okatov, A. Poteryaev, and A. Lichtenstein, cond-mat/0412063 (2004).
- [8] M. Cwik, T. Lorenz, J. Baier, R. Müller, G. André, F. Bourée, F. Lichtenberg, A. Freimuth, R. Schmitz, E. Müller-Hartmann, and M. Braden, Phys. Rev. B **68**, 060401(R) (2003).
- [9] R. Schmitz, O. Entin-Wohlman, A. Aharony, A. B. Harris, and E. Müller-Hartmann, Phys. Rev. B **71**, 144412 (2005); cond-mat/0411583 (2004), Phys. Rev. B (in press).
- [10] B. Keimer, D. Casa, A. Ivanov, J. W. Lynn, M. v. Zimmermann, J. P. Hill, D. Gibbs, Y. Taguchi, and Y. Tokura, Phys. Rev. Lett. **85**, 3946 (2000).
- [11] T. Yildirim, A. B. Harris, O. Entin-Wohlman, and A. Aharony, Phys. Rev. Lett. **73**, 2919 (1994).
- [12] M. Itoh, M. Tsuchiya, H. Tanaka, and K. Motoya, J. Phys. Soc. Jpn. **68**, 2783 (1999).
- [13] J. Akimitsu, H. Ichikawa, N. Eguchi, T. Miyano, M. Nishi, and K. Kakurai, J. Phys. Soc. Jpn. **70**, 3475 (2001).
- [14] T. Hahn (ed.), *International Tables for Crystallography, Vol. A: Space-Group Symmetries* (Dordrecht: Kluwer Academic Publishers, 1995).
- [15] A. Komarek, Diploma thesis, Universität zu Köln (2004).
- [16] P. P. Ewald, Ann. Phys. Leipzig **64**, 253 (1921).
- [17] S. A. Altshuler and B. M. Kozyrev, *Electron Paramagnetic Resonance in Compounds of Transition Elements* (London: Wiley, 1974).
- [18] J. C. Slater, *Quantum Theory of Atomic Structure, Vol. II* (Amsterdam: McGraw-Hill, 1960).
- [19] R. E. Watson, Phys. Rev. **118**, 1036 (1960).
- [20] A. E. Bocquet, T. Mizokawa, K. Morikawa, A. Fujimori, S. R. Barman, K. Maiti, D. D. Sarma, Y. Tokura, and M. Onoda, Phys. Rev. B **53**, 1161 (1996).
- [21] C. Ulrich, A. Gössling, M. Grüninger, M. Guennou, H. Roth, M. Cwik, T. Lorenz, G. Khaliullin, and B. Keimer, cond-mat/0503106 (2005).
- [22] M. Mochizuki and M. Imada, Phys. Rev. Lett. **91**, 167203 (2003).
- [23] W. A. Harrison, *Electronic Structure and the Properties of Solids* (New York: Dover, 1989).
- [24] T. Arima, Y. Tokura, and J. B. Torrance, Phys. Rev. B **48**, 17006 (1993).
- [25] T. Saitoh, A. E. Bocquet, T. Mizokawa, and A. Fujimori, Phys. Rev. B **52**, 7934 (1995).
- [26] R. Rückamp, E. Benckiser, M. W. Haverkort, H. Roth, T. Lorenz, A. Freimuth, L. Jongen, A. Möller, G. Meyer, P. Reutler, B. Büchner, A. Revcolevschi, S.-W. Cheong, C. Sekar, G. Krabbes, and M. Grüninger, cond-mat/0503405 (2005).
- [27] M. W. Haverkort, private communication.
- [28] M. Takahashi, J. Phys. C **10**, 1289 (1977).
- [29] T. A. Kaplan, Z. Phys. B **49**, 313 (1983); L. Shekhtman, O. Entin-Wohlman, and A. Aharony, Phys. Rev. Lett. **69**, 836 (1992).
- [30] G. I. Meijer, W. Henggeler, J. Brown, O.-S. Becker, J. G. Bednorz, C. Rossel, and P. Wachter, Phys. Rev. B **59**, 11832 (1999).